PCCP

PAPER

View Article Online
View Journal

Published on 28 April 2016. Downloaded by University of California - Santa Barbara on 28/04/2016 11:19:50.

Cite this: DOI: 10.1039/c6cp00571c

Unravelling the effect of anchoring groups on the ground and excited state properties of pyrene using computational and spectroscopic methods†

Arunkumar Kathiravan,*[a] Murugesan Panneerselvam,[b] Karuppasamy Sundaravel,[c] Nagaraj Pavithra,[d] Venkatesan Srinivasan,[a] Sambandam Anandan[d] and Madhavan Jaccob*[b]

Received 26th January 2016,
Accepted 8th April 2016

DOI: 10.1039/c6cp00571c

www.rsc.org/pccp

Anchoring groups play an important role in dye sensitized solar cells (DSCs). In order to acquire a suitable anchoring group for DSCs, a deeper understanding of the effect of anchoring groups on the ground and excited state properties of the dye is significant. In this context, various anchoring group connected pyrene derivatives are successfully synthesized and well characterized by using ^{1}H, ^{13}C-NMR, FT-IR and EI-MS spectrometry. The anchoring groups employed are carboxylic acid, malonic acid, acrylic acid, malononitrile, cyanoacrylic acid, rhodanine and rhodanine-3-acetic acid. The optimized geometries, HOMO–LUMO energy gap, light harvesting efficiency (LHE) and electronic absorption spectra of these dyes are studied by using density functional theory (DFT) calculations. The results show that pyrene connected with anchoring groups with weak electron pulling strength (PC, PAC and PMC) has a larger HOMO–LUMO energy gap, whereas that connected with anchoring groups with strong electron pulling strength (PCC, PMN, PR and PRA) has a reduced HOMO–LUMO energy gap. These molecules with a reduced energy gap are primarily preferred for DSC applications. Moreover, P, PC, PAC and PMC molecules undergo $\pi \rightarrow \pi^*$ transition, whereas PCC, PMN, PR and PRA molecules show significant charge transfer along with $\pi \rightarrow \pi^*$ transition. UV-visible absorption spectral studies on these dyes reveal that connecting various anchoring groups with different electron pulling abilities enables the pyrene chromophore to absorb in the longer wavelength region. Notably, an efficient bathochromic shift is observed for PCC, PMN, PR and PRA molecules in both electronic absorption and fluorescence spectral measurements, which suggests that the excitation is delocalized throughout the entire π-system of the molecules. Both theoretical and spectral studies reveal that dyes with an ICT character (PCC, PMN, PR and PRA) are suitable for dye sensitized solar cell applications.

Introduction

Conversion of solar energy into electricity is generally considered to be the most promising way to solve the future energy crisis. Over the past few decades, a large number of light harvesting devices have been developed including dye-sensitized solar cells (DSCs).[1–3] To date, DSC sensitizers based on Ru(II)-polypyridyl complexes have achieved power conversion efficiencies of almost 12% at standard global air mass AM 1.5G.[4,5] However, the large scale application of ruthenium complexes has become a significant problem due to limited resources and the cumbersome purification steps needed. In recent years, interest in organic dyes has increased because of their advantages, such as large molar extinction coefficients, easy modification due to relatively short synthetic routes, and low purification cost, when compared with the conventional ruthenium based chromophores.[6–8] For instance, porphyrins are a family of organic dyes that have fascinating applications in DSCs owing to their extremely high molar extinction coefficients and synthetic versatility.[9–12] In particular, Diau and Grätzel *et al.* have synthesized a push–pull porphyrin (YD2) with a diarylamino moiety as a strong electron-donating group and a carboxyphenylethynyl moiety as a strong electron-withdrawing anchoring group, which exhibited a high η-value of 11%.[13] They further utilized a cobalt(II/III) electrolyte that can yield a higher open circuit voltage (V_{OC}), with a cocktail of a YD2 derivative (YD2-o-C8) and a complementary organic dye to achieve a record η-value of 12.3%.[14] Very recently, a DSC with 13% efficiency was achieved through the molecular engineering

[a] National Centre for Ultrafast Processes, University of Madras, Taramani Campus, Chennai – 600 113, Tamil Nadu, India. E-mail: akathir23@hotmail.com
[b] Department of Chemistry, Loyola College, Chennai – 600 034, Tamil Nadu, India
[c] Chemical Laboratory, CSIR-Central Leather Research Institute, Adyar, Chennai – 600020, Tamil Nadu, India
[d] Nanomaterials and Solar Energy Conversion Laboratory, Department of Chemistry, National Institute of Technology, Tiruchirappalli – 620015, Tamil Nadu, India

† Electronic supplementary information (ESI) available. See DOI: 10.1039/c6cp00571c

Published on 28 April 2016. Downloaded by University of California - Santa Barbara on 28/04/2016 11:19:50.

of SM371 called SM315 (a porphyrin sensitizer).[15] SM315 exhibited significant broadening of Soret and Q-band absorbance features compared to SM371 due to the incorporation of the proquinoidal benzothiadiazole (BTD) unit and it demonstrated an enhancement in green light absorption, resulting in an improved J_{SC} (18.1 *vs.* 15.9 mA cm^{-2} for SM315 and SM371, respectively). Eventually, SM315 achieved 13% power conversion efficiency under full sun illumination without the requirement of a co-sensitizer.

Various organic molecules,[16] such as merocyanine, coumarin, indoline, squaraine, hemicyanine, phenothiazine, triphenylamine, fluorene, carbazole and tetrahydroquinoline have been reported, thus making their application in DSCs desirable. The most efficient metal-free organic dye reported to date has been the phenyldihexyloxy-substituted TPA (DHO-TPA) dye synthesized by Grätzel *et al.*, which exhibits a power conversion efficiency (η) of 10.3% in combination with a cobalt redox shuttle.[17] Wang *et al.* have demonstrated η up to 10.3% for the substituted TPA dye in combination with an iodine/iodide redox shuttle.[18]

The pyrene chromophore is another widely studied building block material due to its durable electronic properties and long lived singlet state.[19,20] In addition, pyrene has multiple substitution sites for molecular engineering.[21] Therefore, many pyrene-based dyes have been developed over the past few decades, and they have been used as a potential candidates for various emerging fields such as organic electronics,[22] fluorescent molecular probes,[23] monomers,[24] triplet sensitizers,[25] sensors,[26] perovskite solar cells[27] and polymer-based solar cells.[28,29] However, DSCs using pyrene-based sensitizers are less common. In 2006, Galoppini *et al.* have reported phenylenethynylene (PE) rigid linkers for TiO_2 sensitization[30] and found that PE rigid linkers convert absorbed photons into electrical current with good efficiency. Later, Thomas *et al.* have reported a series of pyrene-based organic dyes,[31–33] among them a dye containing a terthiophene moiety in the conjugation pathway exhibited a solar energy-to-electricity conversion efficiency of 5.65%.[31] Very recently, Song *et al.* have reported a novel tetrahydropyrene-based D–π–A organic dye,[34,35] which showed a power conversion efficiency of 6.75%. On the other hand, a pyrene-coupled zinc porphyrin shows much improved photovoltaic performance, giving an overall efficiency of 10.06%. This value is superior to that of a N719-based solar cell fabricated under similar experimental conditions (under AM1.5 illumination with an active area of 0.16 cm^2).[36] Although, the power conversion efficiencies of pyrene derivatives are scattered in the literature, to the best of our knowledge there has been no systematic work on the excited state properties of the pyrene derivatives, for instance, the effect of anchoring groups, the π-spacer, aggregation behavior, *etc.* Here, we are interested in examining the effect of various anchoring groups and studying how they affect/improve the characteristics of the pyrene chromophore. Since, dye anchoring is one of the vital processes to achieve high power conversion efficiency, anchoring groups immobilize the sensitizer on the TiO_2 surface and create an interfacial path by which electrons can be transferred from the organic dye to the TiO_2 semiconductor; this process initiates the electrical current in a DSC.[37] Therefore, the nature of the anchoring group to be employed is an important consideration for DSC device functionality.[38] Various anchoring groups have been successfully demonstrated in DSC devices,[39] *e.g.*, carboxylate, phosphonate, sulfonate, salicylate, 8-hydroxyl-quinoline, acetylacetonate, catechol, hydroxyl, pyridyl, hydroxamate, cyanoacrylic acid and rhodanine-3 acetic acid moieties.[40] Carboxylic acid, cyanoacrylic acid and rhodanine-3-acetic acid are found to be efficient electron acceptors and have been widely employed as anchoring groups for the attachment of the visible wavelength absorbing D–π–A dyes on the TiO_2 surface.[41,42]

Even though dyes with various anchoring groups have been reported for DSCs, to the best of our knowledge there are no systematic studies to experimentally probe the effect of anchoring groups on the excited state properties of the dyes. In fact, a minor change in the dye molecular structure will result in different and interesting photophysical, electrochemical and other properties.[43] To gain a deeper insight into the structure–properties relationship of the dye, a series of pyrene derivatives with varying anchoring groups were designed and synthesized. The anchoring groups used were carboxylic acid, malonic acid, acrylic acid, malononitrile, cyanoacrylic acid, rhodanine and rhodanine-3-acetic acid. UV-visible absorption, steady state fluorescence, time resolved fluorescence techniques and computational methods have been used to probe the effect of anchoring groups on the ground and excited state properties of the synthesized dyes (Fig. 1).

Experimental section

Pyrene, pyrene-1-carboxylic acid, pyrene-1-carboxaldehyde, cyanoacetic acid, rhodanine, rhodanine-3-acetic acid and dimethyl sulfoxide-d_6 (DMSO-d_6) were purchased from Sigma-Aldrich. Malonic acid, glacial acetic acid and piperidine were purchased from Sisco Research Laboratories (SRL), India. Malononitrile was purchased

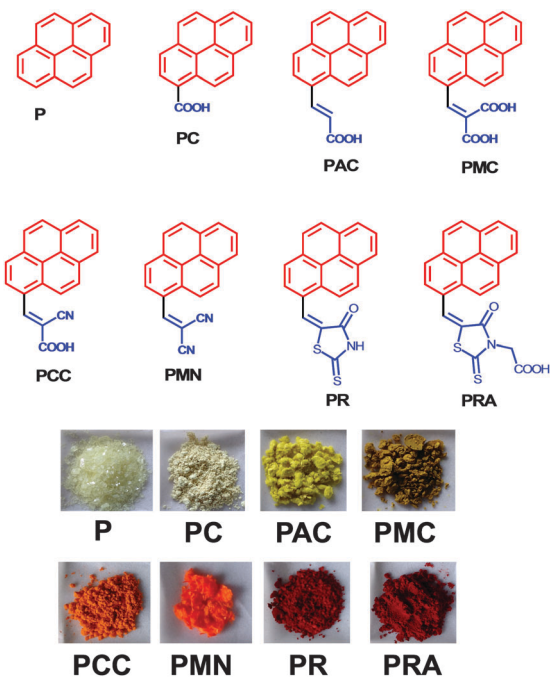

Fig. 1 Structures and photographs of pyrene derivatives.

This journal is © the Owner Societies 2016

Published on 28 April 2016. Downloaded by University of California - Santa Barbara on 28/04/2016 11:19:50.

from Spectrochem and ammonium acetate and tetrahydrofuran were purchased from Qualigens, India and were used without further purification unless otherwise noted. The solvents used for photophysical studies were purchased from Sigma-Aldrich and were of HPLC grade. All measurements were performed in an ambient atmosphere.

Infrared spectrometer (IR) spectra were recorded on a BRUKER VERTEX 70 attenuated total reflection-Fourier transform infrared spectrometer (ATR-FTIR). Nuclear magnetic resonance (NMR) spectroscopy was performed on a BRUKER spectrometer operating at 400 MHz for ^{1}H and 100 MHz for ^{13}C and collected at ambient probe temperature with spectra calibrated using either an internal tetramethylsilane (TMS) standard or a residual protio solvent. Electron ionization-mass spectra (EI-MS) were acquired using a JEOL GC mate-II mass spectrometer photomultiplier tube (PMT) detector. The electronic absorption spectra of samples were recorded using an Agilent 8453 UV-visible diode array spectrophotometer. The fluorescence spectral measurements were carried out using a Fluoromax-4P spectrophotometer (Horiba Jobin Yvon). For fluorescence studies, much diluted solutions were used to avoid spectral distortions due to the inner-filter effect and emission reabsorption. Time resolved picosecond fluorescence decays were obtained by the time-correlated single-photon counting (TCSPC) technique using a microchannel plate photomultiplier tube (Hamamatsu, R3809U) as a detector and a femtosecond laser as an excitation source. The second harmonic (400 nm) output from the mode-locked femtosecond laser (Tsunami, Spectra physics) was used as the excitation source. The instrument response function for the TCSPC system is $\sim$50 ps. The data analysis was carried out by the software provided by IBH (DAS-6), which is based on the reconvolution technique using nonlinear least-squares methods. Femtosecond fluorescence transients have been collected using the fluorescence up-conversion technique. In our femtosecond up-conversion setup (FOG 100, CDP, Russia), the sample was excited using the second harmonic (400 nm) of a mode-locked Ti-sapphire laser (Tsunami, Spectra physics). The fundamental beam (800 nm) was frequency doubled in a nonlinear crystal (1 mm BBO, $\theta = 25^{\circ}$, $\phi = 90^{\circ}$) and used for the excitation. The sample was placed inside a 1 mm-thick rotating quartz cell. The fluorescence emitted from the sample was up-converted in a nonlinear crystal (0.5 mm BBO, $\theta = 38^{\circ}$, $\phi = 90^{\circ}$) using the fundamental beam as a gate pulse. The upconverted light was dispersed in a monochromator and detected using photon counting electronics. The instrument response function of the apparatus was 300 fs. The femtosecond fluorescence decays were fitted using a Gaussian shape for the excitation pulse. The femtosecond fluorescent decay was analyzed by fixing the longer lifetime component obtained from TCSPC.

The fluorescence quantum yield (ϕ_F) of pyrene derivatives[44,45] was calculated by using eqn (1)

$$\phi_F = (A_R/A_S)\,(I_S/I_R)\,(\eta_S/\eta_R)^2\,\phi_R \quad (1)$$

where, subscripts S and R refer to the sample and reference, respectively. A is the absorbance at the excitation wavelength, I is the integrated emission area, and η is the solvent refraction index. Quinine sulphate ($\phi_F = 0.5$)[46] was used as a standard for PC, PAC, PMC and PCC, while fluorescein ($\phi_F = 0.9$)[47] was used as a standard for PMN, PR and PRA.

Quantum chemical calculations were performed using five different functionals such as B3LYP,[48–50] PBE,[50] PBE0,[51,52] M06[53] and ω-b97x-D3[54] with the 6-311+G(d,p) basis set. Among the five functionals, B3LYP is found to predict the energy gap of the pyrene derivatives reasonably. So, we used the B3LYP functional with the 6-311+G(d,p) basis set for performing the TDDFT[55,56] calculations. Harmonic frequency calculations were performed to characterize the stationary points as minima. In order to include the solvent effects, the self consistent reaction field (SCRF) method was performed using polarizable continuum model (PCM) calculations.[57,58] In the present study, a dielectric constant of 7.43 was used to represent the tetrahydrofuran medium. The ground state dipole moment was calculated using the B3LYP functional with the 6-311+G(d,p) basis set. All the DFT calculations were performed using Gaussian 09 software.[59]

FTO glass plates were purchased from BHEL, INDIA. The photoanode[60] was prepared by the following procedure: 0.5 g of TiO_2 (P25) nanoparticles and 0.016 g of polyethylene glycol were added to a solution of 1 M HNO_3. Then, 0.21 ml of acetyl acetone and 0.04 ml of Triton-X were added to the mixture. Later, the mixture was ultrasonicated for 1 h and then stirred for 24 h to get a homogenous TiO_2 paste. Before the preparation of electrodes, FTO plates were washed by sonicating subsequently in a soap solution, distilled water, acetone, and 2-propanol for 15 min. For photoanode preparation, the washed FTO plates were pretreated with 40 mM solution of $TiCl_4$ for 30 min at 70 °C. After $TiCl_4$ treatment, the plates were washed with water and ethanol and then dried at 100 °C on a hot plate for 10 min. Then, the TiO_2 paste was coated on FTO plates using the doctor blade technique. Then, the plates were sintered at 450 °C for 30 min to remove the binder, solvent and achieve an electrically-connected network of TiO_2 particles by sintering in a tubular furnace. After the sintering process, when the temperature of the plates decreased to 80 °C, they were immersed into the dye solution in methanol for 24 h. Excess non-adsorbed dye was washed with anhydrous ethanol. The platinum catalyst counter electrode was prepared by the deposition of $H_2PtCl_6{\cdot}6H_2O$ solution (0.005 M in isopropanol) onto FTO glass and then sintering at 450 °C for 30 min. The DSC devices were fabricated by the following method: the Pt cathode was placed on top of the photoanode and was tightly clipped together. Then, liquid electrolyte 0.05 M I_2/0.5 M LiI/0.5 M 4-tertbutyl pyridine (TBP) in 3-methoxypropionitrile was injected in between the two electrodes. The photocurrent–voltage characteristics and electrochemical impedance spectra (EIS) of the DSCs were measured under 85 mW cm^{-2} light illumination by using an AUTOLAB12/FRA2 electrochemical analyzer. The impedance spectra were recorded in the frequency range from 100 kHz to 1 Hz at their open circuit potential (OCP).

Results and discussion

Molecular design and synthesis

A series of systematically tailored pyrene derivatives were synthesized by Knoevenagel condensation of pyrene-1-carboxaldehyde

Published on 28 April 2016. Downloaded by University of California - Santa Barbara on 28/04/2016 11:19:50.

with the corresponding active methylene group containing compounds in the presence of acetic acid and ammonium acetate as reported elsewhere.[61] The final products were obtained in good yields and successfully characterized by IR, NMR and mass spectroscopic techniques. The synthetic route and characterization data (Fig. S1–S21, ESI†) are described in the ESI† in detail. Taking pyrene (P) and pyrene-1-carboxylic acid (PC) as prototypes, a variety of pyrene-based sensitizers were designed and obtained by incorporating an olefinic bridge (π-bridge which connects the donor and acceptor) with different electron acceptor groups, such as acrylic acid, malonic acid, cyanoacrylic acid, malononitrile, rhodanine and rhodanine-3-acetic acid to tune the HOMO–LUMO energy gap and thus the optical properties of pyrene derivatives. The structures and photographs of the synthesized pyrene-sensitizers are depicted in Fig. 1, which clearly reveal that upon incorporation of strong electron dragging moieties to the pyrene chromophore, the colour of the pyrene derivatives is remarkably intensified, as expected, which is due to the reduced HOMO–LUMO band gaps. From Fig. 1, one can easily understand the impact of anchoring groups on the pyrene chromophore.

Theoretical investigations

Detailed density functional theory (DFT) and time dependent DFT (TD-DFT) calculations were performed to investigate the effect of anchoring groups on the molecular geometry and electron density distribution of pyrene derivatives.[62–64] In order to find a reliable functional for predicting the energy gap (E_s) of the pyrene derivatives, B3LYP, PBE, PBE0, M06 and ω-B97X-D3 functionals were employed. The choice of the best functional was based on the comparison of experimentally determined energy gaps. Energy gap values of pyrene derivatives are presented in Table 1. Different functionals are found to have a greater influence on the calculated energy gap of the pyrene derivatives. It is observed that the long-range corrected ω-B97X-D3 functional is found to overestimate the energy gap of the pyrene derivatives when compared with the experimentally predicted energy gaps. The energy gap of the pyrene derivatives is slightly overestimated when the exchange–correlation hybrid functional PBE0 and meta hybrid generalized gradient approximated (GGA) M06 functionals were employed. Among the two hybrid functionals (B3LYP and PBE), it is clearly observed that the PBE functional is found to underestimate the energy gap values, whereas the B3LYP functional predicts energy gaps closer to the experimentally predicted values with an average difference of 0.29 eV. So the entire manuscript discussion is based on the results obtained at the B3LYP/6-311+G(d,p) level as well as from TDDFT calculations.

Molecular orbital analysis

The optimized structures, along with HOMO and LUMO levels are summarized in Fig. 2. It can be clearly seen from Table 2 that connecting various anchoring groups on the pyrene chromophore eventually reduces the energy gap of pyrene from 3.81 eV to 2.86 eV. The relative order of our computed energy gap (E_s) values is found to have excellent agreement with that of the experimentally calculated energy gap (E_s) values (Table 2).

Table 1 Energy gap (in eV) of frontier molecular orbitals of pyrene derivatives obtained at various levels of theory using the 6-311+G(d,p) basis set in vacuum

Dyes	B3LYP	PBE	PBE0	M06	ω-B97X-D3	Expt.[a]
P	3.81	2.61	4.14	4.20	7.23	3.34
PC	3.52	2.34	3.84	3.93	6.95	3.24
PAC	3.27	2.10	3.60	3.69	6.75	3.07
PMC	3.29	2.06	3.69	3.69	6.79	3.07
PCC	3.05	1.90	3.37	3.46	6.51	2.78
PMN	3.01	1.88	3.32	3.42	6.45	2.63
PR	2.87	1.73	3.17	3.31	6.32	2.59
PRA	2.86	1.72	3.16	3.30	6.34	2.55

[a] Measured in THF.

It clearly shows that the anchoring groups play a vital role in establishing the low energy transition associated with the raised HOMO and the lowered LUMO. Indeed, it is an essential prerequisite for a dye molecule with effective power conversion efficiency and sensitization properties.

From Fig. 2, it is clear that both the HOMO and LUMO are evenly localized on the entire molecule. However, the anchoring groups are found to play a little role in stabilizing the HOMO and LUMO. It is interesting to look into FMOs of PRA where one can notice that the $-CH_2-COOH$ group takes part in neither the HOMO nor the LUMO. But in PMC, the $-CH-(COOH)_2$ group plays a vital role in stabilizing both the HOMO and LUMO. Though the pyrene moiety invariably contributes to the HOMO and LUMO, its contribution is diminished towards the LUMO. For instance, in PMN, the participation of the dicyano substituted vinyl moiety stabilizes the LUMO significantly compared to the pyrene unit. Similarly in the case of PR and PRA, the

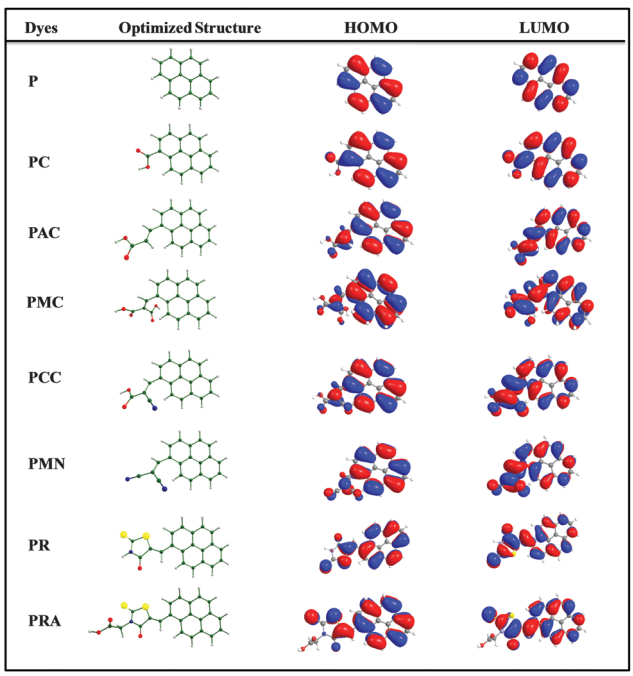

Fig. 2 Optimized structures and electron distributions at HOMO/LUMO levels of the pyrene derivatives.

This journal is © the Owner Societies 2016

Published on 28 April 2016. Downloaded by University of California - Santa Barbara on 28/04/2016 11:19:50.

Table 2 Photophysical properties of pyrene derivatives in THF medium (derived from both #experimental and *computational methods)

	Pyrene derivatives							
Parameters	P	PC	PAC	PMC	PCC	PMN	PR	PRA
#Expt. λ_{abs} (nm)	336	353	367	367	383	438	442	452
*TDDFT λ_{abs} (nm)	345	381	422	436	471	478	499	503
#log ε	4.85	4.42	4.48	4.18	4.20	4.36	4.56	4.54
#λ_{emi} (nm)	393	406	420	420	479	501	513	517
*λ_{emi} (nm)	377	413	421	436	471	478	537	540
#E_s (eV)	3.34	3.24	3.07	3.07	2.78	2.63	2.59	2.55
#E_{ox} (V)	—	—	—	—	1.42	1.46	1.30	1.30
#E_{ox}* (V)	—	—	—	—	−1.36	−1.17	−1.29	−1.25
#ΔG_{inj} (eV)	—	—	—	—	−0.86	−0.67	−0.79	−0.75
#ΔG_{rec} (eV)	—	—	—	—	−1.92	−1.96	−1.80	−1.80
#ϕ_F	0.75[a]	0.3	0.5	0.5	0.004	0.003	0.002	0.002
#τ (ns)	10	7.9	3.0	3.0	<0.05	<0.05	<0.05	<0.05
*HOMO (eV)	−5.67	−5.96	−5.84	−5.90	−6.04	−6.20	−5.92	−5.89
*LUMO (eV)	−1.86	−2.44	−2.57	−2.61	−2.99	−3.19	−3.05	−3.03
*E_s (eV)	3.81	3.52	3.27	3.29	3.05	3.01	2.87	2.86
*Transition	π → π*	π → π*	π → π*	π → π*	π → π* + ICT	π → π* + ICT	π → π* + ICT	π → π* + ICT
*% of transition	92.5	95.2	98.0	95.2	98.0	98.0	98.0	98.0
*f	0.41	0.51	0.61	0.43	0.47	0.48	0.93	0.97
*LHE	0.61	0.69	0.75	0.63	0.66	0.67	0.88	0.89

[a] From ref. 44.

presence of the rhodanine group stabilizes the LUMO effectively through the vinyl bridge which favours significant charge transfer along with the π → π* transition. The computed results show that the HOMO and LUMO of all the molecules are π and π* orbitals, respectively. This gives some information on their electronic transitions which mainly originate from the π → π* transition along with the charge-transfer (CT) character. This shows that P, PC, PAC and PMC molecules possess the π → π* transition, whereas PCC, PMN, PR and PRA molecules show π → π* transition along with intramolecular charge transfer (ICT).

It is noteworthy to analyze and understand the origin of the individual contributions of various segments of the dye molecules towards the HOMO and LUMO levels. So, the Chemissian program was used to compute the individual contributions of various fragments of the dyes (Table S1, ESI†). The whole molecule was segmented into two fragments, namely the pyrene unit and the anchoring group. From Table S1 (ESI†), it is clear that the majority of the HOMO electron density is concentrated on the pyrene unit and the contribution of the acceptor group increases largely in the LUMO level by changing the anchoring group from diacetic acid to rhodanine acetic acid thereby significantly reducing the contribution of the pyrene unit. It is illustrated that changing the specific substituent on the pyrene ring facilitates the effective intramolecular charge transfer to the acceptor group. Therefore, HOMO–LUMO transitions of the above molecules (PCC, PMN, PR and PRA) bear a significant ICT nature along with the π–π* transition. In the case of PRA, the contribution of donor and acceptor groups to the HOMO level is 81% and 19%, respectively, whereas the LUMO is localized on both donor and acceptor groups (55% and 45%, respectively). It clearly indicates that the rhodanine acetic acid group in PRA facilitates effective charge transfer.

In all the above cases, apart from P, there is a significant electronic density on the anchoring groups. This is a favorable feature to enhance the effective electronic coupling of the excited state with the wave function of the TiO_2 conduction band. In the case of PCC, PMN, PR and PRA, there is a significant electron density on the acceptor moieties and this property shows that these molecules are effective candidates for DSCs. In addition, the E_{LUMO} values (Scheme 1) of pyrene derivatives were located above the conduction band edge (E_{cb}) of TiO_2 (−4.0 eV *vs.* vacuum), while the E_{HOMO} values were below the energy of the redox species of iodide/triiodide (−4.8 eV *vs.* vacuum).[65] From these values, we have concluded that the relative matching of electronic levels of sensitizers would lead to energetically favorable electron injection as well as regeneration of oxidized dyes during DSC operation.

Computed absorption spectra of pyrene derivatives

In order to rationalize the absorption spectra of the pyrene derivatives in THF continuum, we employed TDDFT calculations

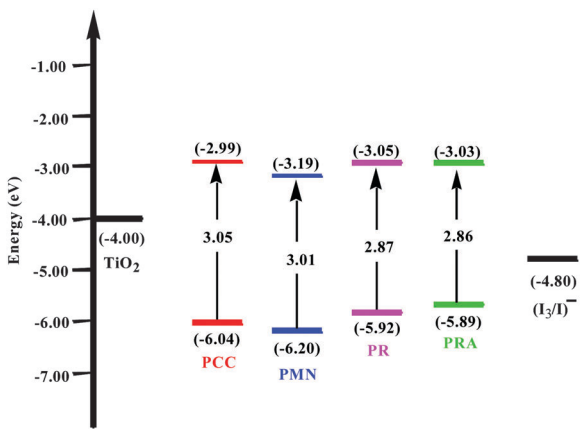

Scheme 1 HOMO/LUMO energy levels of the pyrene derivatives.

Published on 28 April 2016. Downloaded by University of California - Santa Barbara on 28/04/2016 11:19:50.

using four different DFT functionals such as B3LYP, PBE, M06 and ω-b97x-D3. Table S2 (ESI†) summarizes the absorption maxima obtained from the different functionals along with experimental absorption λ_{max} values. Among the functionals, the long-range and dispersion corrected ω-b97x-D3 functional is found to underestimate the λ_{max} value compared with the experimental value. A larger deviation from the experimental λ_{max} value is found using the PBE functional. Both B3LYP and M06 functionals were found to predict the λ_{max} value of pyrene derivatives closer to the experimental values. The absorption bands computed using both the functionals are found to have the same trend as that of experimental values. In the present study, the B3LYP functional is used to discuss the absorption spectra of pyrene derivatives. So, the calculated absorption maxima, level of electronic transitions, excitation energies (eV) and oscillator strengths for the most relevant singlet excited states of pyrene derivatives obtained from the B3LYP functional are summarized in Table 2. Moreover, upon moving from simple pyrene to pyrene derivatives with different anchoring groups, a promising bathochromic shift was observed. For instance, the dominant absorption band of simple pyrene (P) is found at 345 nm (3.59 eV), whereas for PRA it is found at 503 nm (2.46 eV). The reduction in the energy gap from P to PRA is also accompanied by an increase in the oscillator strength. This clearly suggests that the oscillator strength of the dye molecules is easily tuned by varying the electron pulling strength of the acceptor moieties. From the molecular orbital analysis, the dominant absorption bands for P to PMC are primarily due to $\pi \rightarrow \pi^*$ transition. The nature of electronic transition is changed when we substitute the strong electron withdrawing groups such as cyano and rhodanine groups. By visualizing the molecular orbitals, the dominant absorption bands of PR and PRA molecules are due to the intramolecular charge transfer (ICT) along with $\pi \rightarrow \pi^*$ transitions. Interestingly, introducing the rhodanine moiety in the pyrene ring not only increases the absorption maxima but also increases the intensity of ICT transition along with the $\pi \rightarrow \pi^*$ transition. This is exactly consistent with the conclusions arrived at from FMO analysis. The computed λ_{max} for pyrene derivatives with different anchoring groups has the following order: P < PC < PAC < PMC < PCC < PMN < PR < PRA. The above order is in good agreement with experimentally predicted λ_{max} for pyrene derivatives.

In addition, we have measured theoretical emission spectra of pyrene derivatives using the B3LYP functional. We found that our computed emission spectra are in good agreement with the experimental emission spectra of pyrene derivatives (Table 2). The observed trends in the absorbance and emission spectra of pyrene derivatives suggest that the excitation is delocalized throughout the entire π-system of the molecules. From the above results, one can conclude that substitution of selective electron withdrawing groups on the pyrene ring strongly influences the nature of electronic transitions.

Natural transition orbital analysis

In addition to the above, we have also performed the natural transition orbital analysis (NTO) to confirm the nature of electronic transitions in pyrene derivatives.[66] It is calculated based on the transition density matrices and used to represent the transition density between unoccupied electron transition orbitals and occupied hole transition orbitals. One should not confuse them with the occupied and unoccupied molecular orbitals obtained from simple ground state calculations. The natural transition orbitals (NTOs) for pyrene derivatives are given in Fig. 3. The NTO corresponds to the absorption bands of P, PC, PAC and PMC shows a characteristic $\pi \rightarrow \pi^*$ transition. In the case of PMN, PCC, PR and PRA, NTOs possess an ICT nature along with the $\pi \rightarrow \pi^*$ transition. This effect is much more pronounced in the PR and PRA molecules. The strong ICT nature of PR and PRA was confirmed through the higher electronic NTO contribution of the rhodanine part in PR and PRA molecules. It is consistent with the results obtained from the FMO analysis. Based on the NTO analysis, effective intramolecular charge transfer along with the $\pi \rightarrow \pi^*$ transition can be expected in the case of PR and PRA molecules due to the presence of the strong electron withdrawing rhodanine group.

Dipole moment

In structural chemistry, the variation of the electronic charge distribution in the molecules is directly inferred from the ground state dipole moment values. The electronic charge distribution is greatly affected even by a subtle change in the structure of the molecule.

The calculated ground state dipole moments of the pyrene derivatives in both gas phase and THF medium at the B3LYP/6-311+G(d,p) level are summarized in Table S3 (ESI†). Due to the presence of a moderately polar solvent, the dipole moment computed in solvent is slightly higher than the dipole moment computed in the gas phase. However, in both gas and THF medium, the trend in the computed dipole moment is similar. The polarity of the simple pyrene molecule significantly increases by the introduction of different electron withdrawing groups. The charge separation significantly enhances through the introduction of cyano and rhodanine groups in pyrene (PCC, PMN, PR and PRA). Among all the molecules, PMN is found to have a large dipole moment value due to the presence of two highly polar cyano groups in PMN (9.4 Debye). As we discussed in earlier sections, effective intramolecular charge transfer can be expected in the case of PMN, PCC, PR and PRA molecules.

Light harvesting efficiency

The light harvesting efficiency (LHE)[67] is one of the important parameters related to the intensity of the absorption spectra of the dye molecule and is calculated using eqn (2),

$$\mathrm{LHE} = 1 - 10^{-f} \quad (2)$$

where, f is the oscillator strength of the dye molecule. For an efficient photocurrent response, the LHE of the dye molecule should be high. The calculated LHE values for $S_0 \rightarrow S_1$ bands of the dye molecules are given in Table 2. It evidently shows

 This journal is © the Owner Societies 2016

Published on 28 April 2016. Downloaded by University of California - Santa Barbara on 28/04/2016 11:19:50.

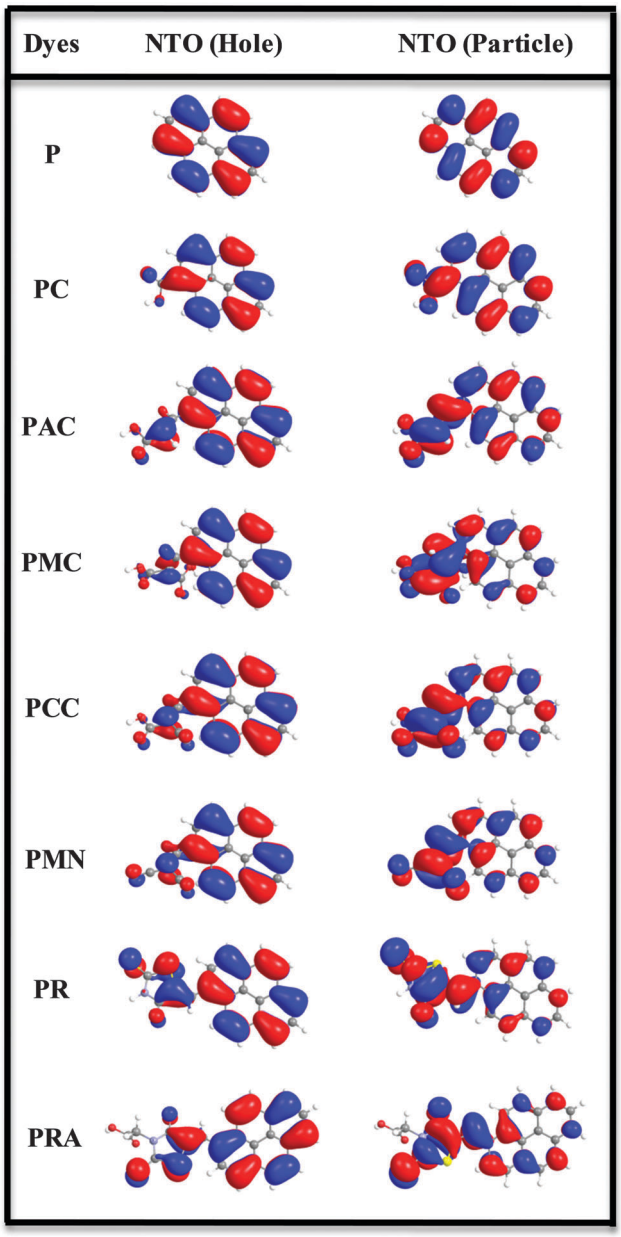

Fig. 3 Natural transition orbitals (NTOs) of pyrene derivatives shown on occupied (holes) and unoccupied (electrons) NTO pairs.

that PRA is found to have better LHE properties than the rest of the molecules. However, the LUMO in PRA does not extend its carboxylate group that links the dye to the TiO_2 surface, indicating less electronic coupling between the dye LUMO and the acceptor states of TiO_2. In the case of other dye molecules such as PCC, PMN and PR, conjugation is extended to the acceptor moiety. Based on our calculations, PCC, PMN, PR and PRA are found to be excellent candidates for DSCs, since they show effective charge separation between the HOMO and the LUMO induced by light excitation. In spite of this, it is expected that the electrons which are generated upon photoexcitation of the pyrene derivatives anchored onto the TiO_2 surface can be successively transferred from the donor to the electron acceptor and finally to the conduction band of TiO_2.

Absorption characteristics

The light harvesting efficiency of the dye in the photoanode is the most important and indispensable factor for the high-efficiency of a DSC, which is mainly related to the molar extinction coefficient of the sensitizer, dye-loading capacity in the electrode and the optical path of the incident light in the electrode. Consequently, the light harvesting efficiency is primarily governed by the molar extinction coefficient of the dye.[68] Hence, the UV-vis absorption spectra of the pyrene derivatives were recorded in THF and are shown in Fig. 4. It can be seen that by varying anchoring/acceptor groups, the absorption spectra of pyrene derivatives extended to the visible region compared with that of unsubstituted pyrene. Intriguingly, PC, PAC and PMC show a moderate bathochromic shift, whereas PCC, PMN, PR and PRA exhibit a remarkable bathochromic shift. These results clearly show that cyano acrylic acid, malononitrile, rhodanine and rhodanine-3-acetic acid have a stronger electron accepting tendency than carboxylic acid, acrylic acid and malonic acid.

Typically, pyrene molecules are very prone to form aggregates in solution.[69] Therefore, we intend to investigate the aggregation behaviour of the pyrene derivatives in THF solvent. Upon increasing the concentration of pyrene derivatives, the absorbance increased linearly and no new bands were observed.

At the same time, Beer–Lambert's law was obeyed in the concentration range from 10 μM to 50 μM. This shows that the pyrene derivatives are not significantly aggregated within the above mentioned concentration range (spectra are not shown here) and the molar absorption coefficients (ε) of pyrene derivatives are listed in Table 2. The measured ε values are found to be larger than that of Ru-complex photosensitizers,[70] suggesting that these molecules can convert the visible light energy to electrical energy in an effective manner. The absorption band appearing in the ultraviolet region corresponds to the $\pi \rightarrow \pi^*$ transition, while the other, covering the visible region, can be assigned to the intramolecular charge transfer (ICT) process.[71] Therefore, we assigned the ICT transition to PCC, PMN, PR and PRA molecules and the $\pi \rightarrow \pi^*$ transition to P, PC, PAC and PMC.

To address the ICT transition in a detailed manner, two structurally similar candidates such as PMC and PCC were considered here. PMC shows an absorption band at 367 nm and PCC shows a maximum absorption band at 383 nm and a moderate band at 415 nm. The latter shows a significant bathochromic shift compared with PMC, due to the intra-molecular charge transfer between the pyrene donor and the cyanide (–C≡N) electron acceptor. It is also important to monitor the color differences between these two molecules; PMC shows a light yellow color, whereas PCC possesses an orange color. This is an excellent support for the supposition that PCC is mainly due to ICT. The presence of ICT in PCC is further established by the addition of triethylamine (TEA) to the PCC solution. Based on the earlier reports,[72,73] TEA partially deprotonates the carboxylic acid in the ground state.

Published on 28 April 2016. Downloaded by University of California - Santa Barbara on 28/04/2016 11:19:50.

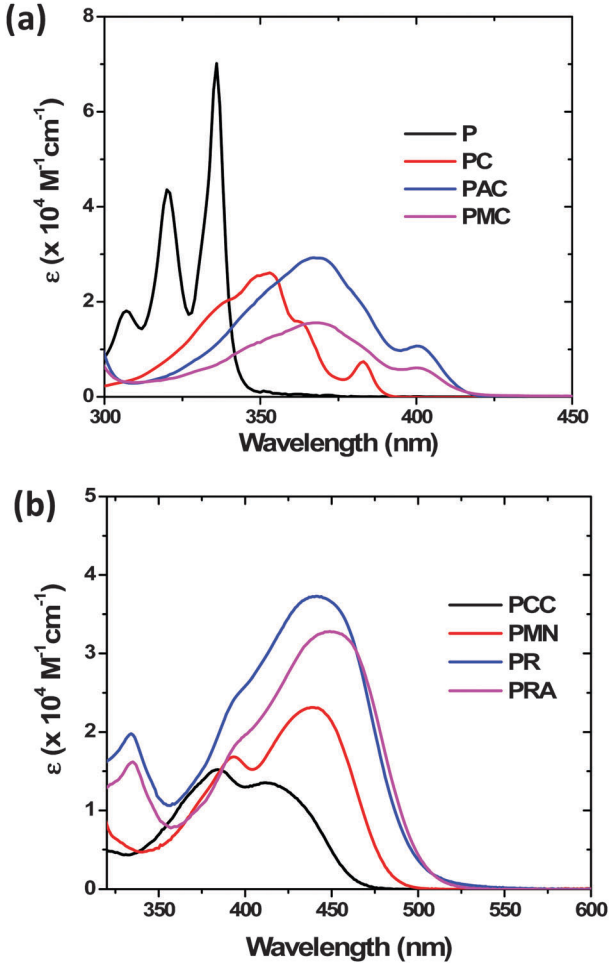

Fig. 4 UV-vis absorption spectra of pyrene derivatives in THF. (a) $\pi \rightarrow \pi^*$ character (b) ICT character.

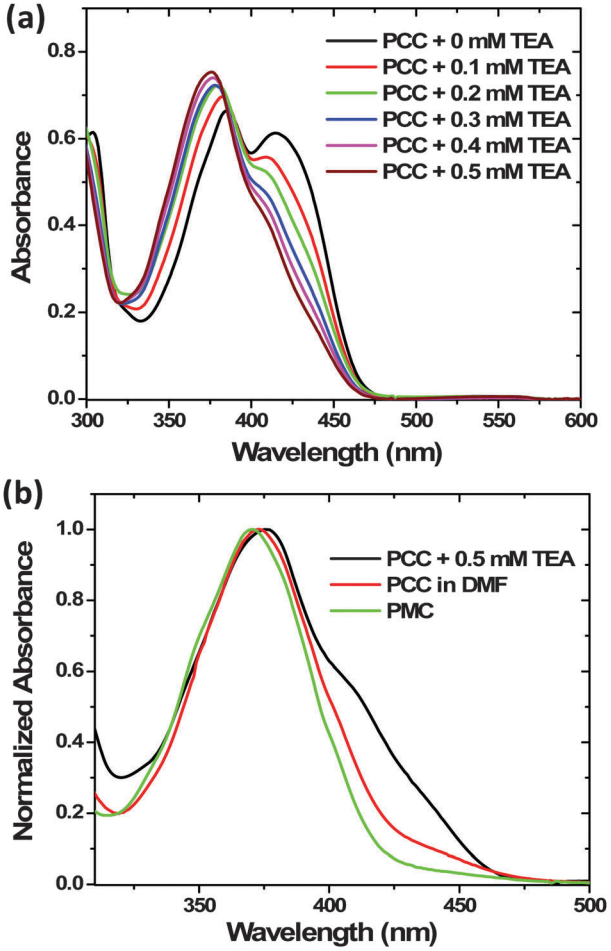

Fig. 5 Absorption spectra of PCC (a) with varying TEA concentrations (b) in 0.5 mM TEA, in DMF and PMC in DMF.

As a result, it would diminish the electron-accepting strength of the acceptor moiety (–C≡N), which in turn may significantly decrease the donor–acceptor interaction in the dye, which will lead to a hypsochromic shift in the absorption spectrum.[74] Here, we employed the same strategy to establish the ICT character of PCC.

Upon addition of TEA to the solution of PCC, the absorption band at 415 nm decreases with a simultaneous hypsochromic shift at 383 nm(Fig. 5a). The decrease of the ICT band is due to the deprotonation of carboxylic acid by TEA which leads to the decrease in the electron accepting strength of the –C≡N group. This new absorption band observed is nearly similar to the absorption band of PMC (Fig. 5b). However, in the case of PMC, upon addition of TEA, there is no significant change in the absorption spectrum (spectra not shown here). Further, the formation of hydrogen bonding interaction between the solvent and the carboxylic acid group of the dye will also reduce the acceptor strength of the –C≡N group, eventually shifting the absorption spectrum to the lower-wavelength region. Hence, we envisioned to measure the absorption spectrum of PCC in DMF solvent, where the observed spectral behavior of PCC in DMF is quite similar to the spectrum of PCC in 0.5 mM TEA and PMC (Fig. 5b). The spectral data clearly indicate that the introduction of a –C≡N group induces the ICT character in PCC which is sensitive to the surroundings. Furthermore, upon introduction of one more –C≡N group in PCC (*i.e.* PMN), enhancement of the intensity of color is observed. Obviously, the dicyanomethylene group is a strong electron acceptor and shows an intense color due to the strong interfacial charge transfer properties.[75] Similarly, we also perceived color changes from orange to deep-orange on moving from PCC to PMN, this supports the ICT.

Also, it is found in the literature that the rhodanine[76] moiety exhibits a stronger electron withdrawing ability with concomitant widening of the absorption spectral response compared to cyanoacrylic acid. Accordingly, upon replacing the cyanoacrylic acid in PCC by the rhodanine moiety as in PR, a significant bathochromic shift is observed, which clearly shows that the rhodanine moiety has a strong tendency to accept electrons from the pyrene chromophore. Further, there is no significant change in the absorption spectra of PR and PRA. In both cases, the LUMO is mainly concentrated on the rhodanine unit, especially on the carbonyl and thiocarbonyl groups. However, in the case of PRA, breaking of the conjugation between the

This journal is © the Owner Societies 2016

Published on 28 April 2016. Downloaded by University of California - Santa Barbara on 28/04/2016 11:19:50.

rhodanine unit and the carboxylic acid group is instigated by the presence of the methylene group in rhodanine-3-acetic acid.

Perhaps, the most striking result of the UV-visible absorption spectral studies is that connecting various anchoring groups with different electron pulling capacities induces the pyrene chromophore to absorb at longer wavelengths. Interestingly, the order of magnitude (10^4) of molar extinction coefficients does not vary significantly within the pyrene series. Indeed, among the pyrene-sensitizer scrutinized, PRA is superior to the other molecules on the basis of light harvesting ability.

Fluorescence characteristics

To explore the effect of anchoring groups on the pyrene excited state, the fluorescence spectra of pyrene derivatives were recorded in THF medium and all the samples were excited at their absorption maximum (Table 2). Pyrene molecules are very prone to form an excimer in the excited state,[77] however, this can be avoided by using very dilute solutions. Hence, all the samples were measured under highly dilute conditions (10^{-6} M). The normalized fluorescence spectra of pyrene derivatives are shown in Fig. 6. Similar to absorption spectra, a bathochromic shift was observed in fluorescence spectral studies. The observed bathochromic shift in the absorbance and fluorescence spectra of pyrene derivatives suggest that the excitation is delocalized throughout the entire π-system of the molecules. Moreover, besides the π → π* character, the pyrene derivatives with the ICT character display a weak fluorescence in solution. It is well known that the ICT is a competitive relaxation process of the singlet excited state and typically reduces the fluorescence.[78]

In the π → π* character dyes, an interesting behaviour in the fluorescence spectra of PAC and PMC was observed. Both molecules show very similar fluorescence spectra with two pronounced peaks at 420 nm and 438 nm. To determine whether these candidates have dual emission properties or not, we have measured the excitation spectra of these dyes. The excitation spectra at both emission wavelengths are almost the same, which confirms that these two peaks arise from the same electronic excited state. Notably, the obtained excitation spectra are quite similar to the absorption spectra (Fig. S22, ESI†). In addition, we have recorded the fluorescence spectra of PAC and PMC in DMSO (high viscous solvent) and observed a single emission peak at 438 nm and this indeed indicates that the observed peaks in THF (low viscous solvent) are not due to dual emission (Fig. S23, ESI†). In addition, the time resolved fluorescence measurements were also performed to verify the dual emission properties of these molecules. The emission monitored at both wavelengths gave similar decays, which evidently preclude the question of dual emission properties. Moreover, both the molecules show very similar single exponential [$F(t) = A\exp(-t/\tau)$] fluorescence decays with a lifetime of 3 ns and they exhibit similar fluorescence quantum yields; it clearly suggest that the additional carboxyl group does not influence the excited state character noticeably relative to that of PAC.

As mentioned earlier, dyes with strong electron withdrawing groups (PCC, PMN, PR and PRA) show very weak fluorescence in solution, due to ICT. Further, to demonstrate the ICT

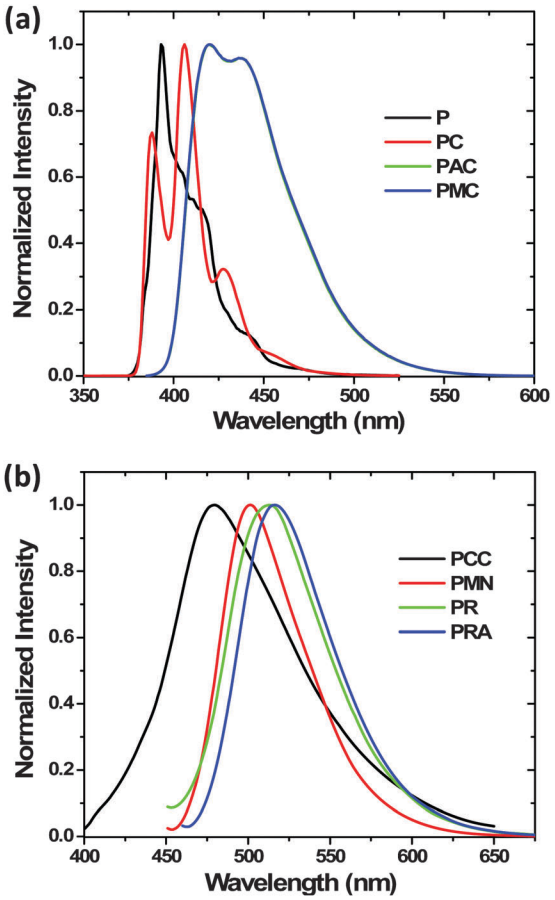

Fig. 6 Fluorescence spectra of pyrene derivatives in THF. (a) π → π* character (b) ICT character.

character in the excited state, we have selected two ideal candidates such as PMC and PCC. On close examination of the fluorescence properties of these molecules (Fig. 7a), PMC shows a strong fluorescence and PCC shows a very weak fluorescence in equiabsorbing solutions. Moreover, the fluorescence quantum yields were dropped from 0.5 (PMC) to 0.001 (PCC). Fluorescence quenching of PCC is due to ICT (*cf.* above). This phenomenon is further verified by using time resolved fluorescence spectroscopy. Fig. 7b shows the time resolved fluorescence decay of PCC and PMC in THF solution. The fluorescence decay of PMC is fitted with a single exponential function with a lifetime of 3 ns, however, the decay of PCC is almost as fast as our laser instrument response (50 ps).

However, the same dye (PCC) measured in DMF shows single exponential fluorescence decay; because the hydrogen bonding of the carboxylic acid group of the dye with the solvent reduces the acceptor strength of the $-C\equiv N$ group, the ICT character of PCC is diminished. It is also interesting to note that the fluorescence decay of PCC and PMC in DMF is very similar. Indeed, this indicates that the ICT character of the PCC dye completely disappears in DMF solvent. The other ICT dyes namely PMN, PR and PRA also exhibit weak fluorescence in solution. The fluorescence decays of these dyes are also fast (<50 ps), and no fitting could be obtained (Fig. 8a).

Published on 28 April 2016. Downloaded by University of California - Santa Barbara on 28/04/2016 11:19:50.

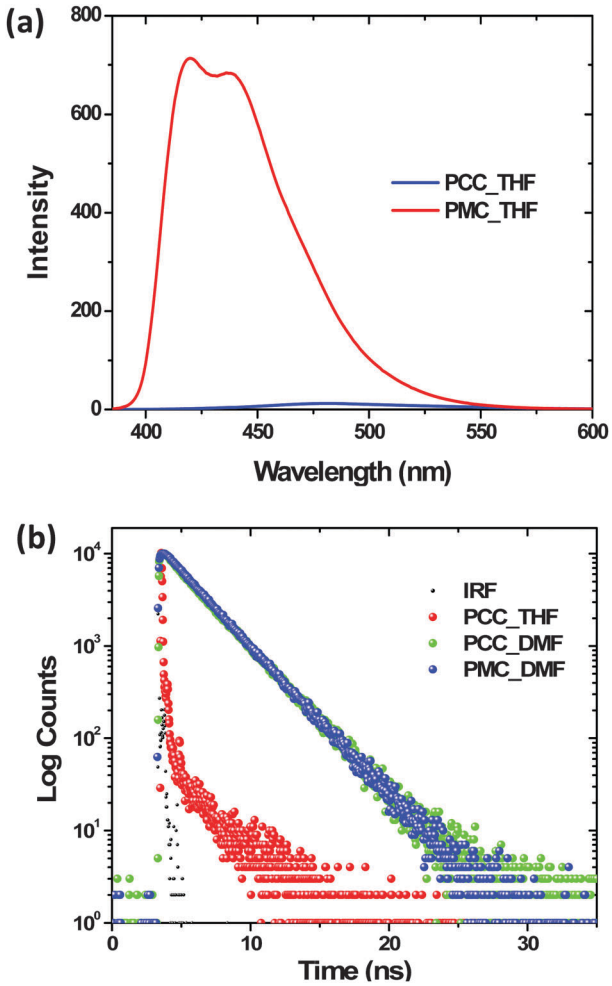

Fig. 7 (a) Fluorescence spectra of PCC and PMC in THF at equiabsorbing solutions. (b) Time resolved fluorescence decay of PCC and PMC. (λ_{ex} = 400 nm).

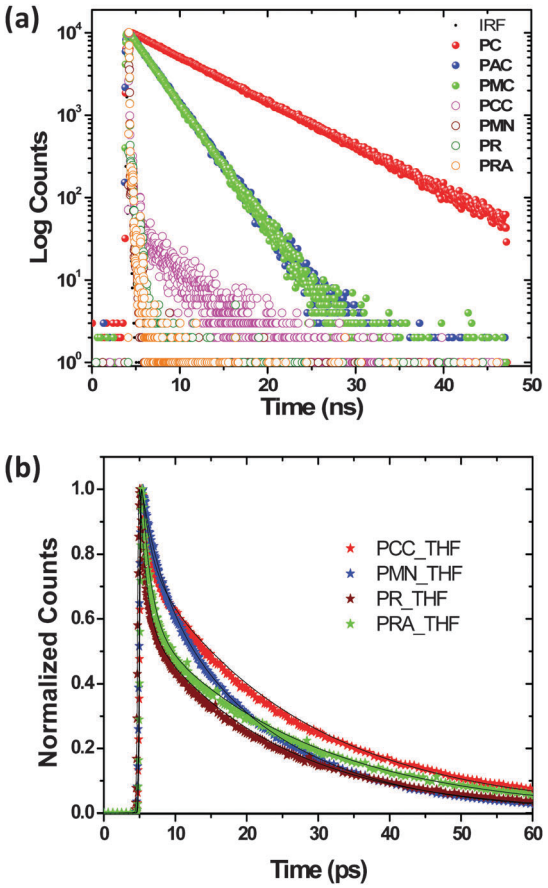

Fig. 8 (a) Time resolved fluorescence decay of pyrene derivatives in THF. (b) Femtosecond fluorescence decay of ICT dyes. (λ_{ex} = 400 nm).

Table 3 Fitting parameters of pyrene derivatives in THF

Dyes	τ_1 (ps)	τ_2 (ps)	A_1 (%)	A_2 (%)	τ_{av} (ps)
PCC	1.3	22.4	28	72	16.4
PMN	2.8	16.63	27	73	12.8
PR	0.96	18.7	49	51	10
PRA	1.3	23.08	48	52	12.6

Hence, a femtosecond-fluorescence setup was used to extract the lifetime of the ICT dyes. Fig. 8b displays the femtosecond (fs) fluorescence decays of ICT dyes in THF medium, measured in a 60 ps time window upon excitation at 400 nm. The fluorescence decay of these dyes is recorded at their emission maximum. The obtained fluorescence decays were fitted with a biexponential function and the fitted values are collected in Table 3. The ultrafast decay component, τ_1 is attributed to the solvation relaxation of the excited states and τ_2 is due to the lifetime of the relaxed charge transfer state. The average lifetime of the ICT dyes is about ~10 ps. For an efficient device, the requirement of an electron injection process at the photoanode (*i.e.* dye to TiO_2) should be very fast (10 fs to 150 fs) relative to the excited state decay to the ground state (10 ns). For instance, the electron injection process of the most successful N3 dye[79] occurred between 10 to 150 fs time scales, which are faster than the excited state lifetime decay to the ground state (60 ns).[70] Hence, the observed excited state lifetime for pyrene derivatives hopefully favours the electron injection process at the TiO_2 surface, before they relax to the ground state.

To thermodynamically judge the possibility of electron transfer from the excited dye to the conduction band of TiO_2, cyclic voltammetry and differential pulse voltammetry (DPV) measurements were performed to determine the oxidation potentials of the dyes (Fig. S24, ESI†). The measurements were carried out using a typical three-electrode electrochemical cell, which consists of a glassy carbon electrode which is used as the working electrode, while platinum wire and Ag/AgCl were used as the counter and reference electrodes, respectively. All of the dyes show an oxidation wave which is attributable to the removal of an electron from the pyrene segment. The exact oxidation potentials of the pyrene derivatives were calculated using the DPV method and are listed in Table 2. As shown in this table, the first oxidation potentials (E_{ox}) correspond to the HOMO levels of the dyes, which are more positive than the redox potential of the $(I/I_3)^-$ redox couple (0.4 V), indicating

This journal is © the Owner Societies 2016

Published on 28 April 2016. Downloaded by University of California - Santa Barbara on 28/04/2016 11:19:50.

that reduction of the oxidized dyes with I^- ions is thermodynamically feasible. On the other hand, the excited state oxidation potentials (E_{ox}*), which correspond to the LUMO levels of the dyes can be obtained using eqn (3):

$$E_{ox}^* = E_{ox} - E_{(0-0)} \quad (3)$$

where, $E_{(0-0)}$ is the excited state energy of the dye, which is estimated from the intersection between the normalized absorption and emission spectra. The obtained E_{ox}* of the dyes are more negative than the conduction band potential of TiO_2 (−0.5 V *vs.* NHE), indicating that the electron injection process from the excited dyes to the TiO_2 conduction band is energetically favourable.

Driving forces for electron injection (ΔG_{inj}) from the dye excited state to the CB of TiO_2 and electron recombination (ΔG_{rec}) from the CB of TiO_2 to the dye radical cation (E_{ox}) are determined from the following equations and the values are shown in Table 2.

$$\Delta G_{inj} = E_{ox}^* - E_{CB} \quad (4)$$

$$\Delta G_{rec} = E_{CB} - E_{ox} \quad (5)$$

The obtained ΔG values are negative, which indicates that both of the processes are thermodynamically feasible and most importantly injection is the dominant process compared to recombination for these dyes.

The main motivation of this work is to perceive how anchoring groups influence the ground and excited state properties of the pyrene chromophore. In addition, it is worth pursuing this molecule at the application level. Hence, TiO_2 sensitization and *I–V* measurements are carried out. The results are presented below.

Dye adsorption in various solvents

According to the literature, dyes in various solvents exhibit diverse interactions with the solvents, which could alter the physical and chemical interactions between dyes and the TiO_2 surface.[80] Therefore, optimization of the solvents for TiO_2 sensitization is very important for obtaining good conversion efficiency (η) in DSCs.[81] For this reason, we have selected methanol, DMF and THF as solvents. It is noticed that, among the synthesized dyes, PCC and PRA adsorb well on the TiO_2 surface. Although, nitrile and imide groups are reported as anchors for TiO_2.[81] However, in our case PMN and PR does not adsorb on the TiO_2 surface under ideal conditions. PC, PAC and PMC molecules absorb in the same region where TiO_2 absorbs, hence, no sensitization is carried out. In order to optimize the solvents for TiO_2 sensitization we have chosen the visible light active PRA molecule. While optimizing the solvents for TiO_2 sensitization, one has to prepare identical dye/TiO_2 films in a particular solvent. Keeping this in mind, we have prepared three PRA/TiO_2 films under identical conditions, *i.e.*, dye concentration (2×10^{-4} M), sensitization time (1 h) and sensitization solvent (MeOH). The UV-vis absorption spectra of all the PRA/TiO_2 films show similar absorption, no broadening and enhancement of the spectra are observed with respect to the prepared films (Fig. S25, ESI†). This clearly shows that whenever we prepare the dye/TiO_2 films under identical conditions we reproduce a similar surface coverage. Now, we turn back to the main objective of this section, *i.e.*, the effect of solvents on the dye/TiO_2 interface. Fig. S26 (ESI†) shows the UV-vis absorption spectra of PRA and PRA/TiO_2 films in various solvents. The absorption spectra of PRA do not vary too much by varying solvents. However, there is a significant effect on the adsorption process. The absorbance of the PRA/TiO_2 films in methanol solvent is very high compared with DMF and THF solvents. Moreover, it is interesting that a large amount of PRA is adsorbed on the TiO_2 surface in methanol solvent. Thus, the protic solvents strongly influence the adsorption of the PRA on the TiO_2 surface. This result, clearly suggests that the selection of appropriate solvents plays a key role in improving the photoanode of a cell. Hence, we have selected methanol as a suitable solvent for making the photoanode, *i.e.*, dye/TiO_2 films.

Moreover, the fluorescence emission band disappears when the dye is adsorbed onto a TiO_2 film. This phenomenon can be explained by the efficient electron injection from the excited singlet state of the dye to the conduction band of TiO_2 and suggests that both dyes (PCC and PRA) are good sensitizers on TiO_2 films.

Photovoltaic performance

In order to investigate the impact of anchoring groups on solar cell performance, we have preferred PCC and PRA dyes, since these two candidates adsorb well on the TiO_2 surface (Fig. S27, ESI†). The *J–V* curves of DSCs based on pyrene sensitized electrodes under simulated AM 1.5 irradiation (85 mW cm^{-2}) are shown in Fig. 9. The electrolyte was composed of 0.05 M I_2/0.5 M LiI/0.5 M 4-*tert*-butylpyridine (TBP) in 3-methoxypropionitrile. The measured open-circuit photovoltage (V_{OC}), short-circuit photocurrent density (J_{SC}), fill factor (FF) and solar-to-electric conversion efficiencies (η) are listed in Table 4. PCC and PRA sensitized solar cells give short-circuit photocurrent densities (J_{SC}) of 2.11 and 0.83 mA cm^{-2}, open circuit voltages (V_{OC}) of 0.63 and 0.47 V, and fill factors (FF) 0.53 and 0.50, corresponding to the overall conversion efficiencies (η) of 0.84% and 0.23%, respectively. Evidently, PCC shows better solar cell performance than PRA, especially in terms of J_{SC} and V_{OC}. This can be explained on the basis of electron injection and surface coverage properties. The LUMO of the PCC is largely populated on the acceptor moiety, however for PRA it is mainly located on the rhodanine moiety and it does not extend its carboxylate group that links the dye to the TiO_2 surface, indicating a less strong electronic coupling between the dye LUMO and the acceptor states of TiO_2. However, in the case of the PCC dye, conjugation is extended to the carboxylic group that leads to efficient electron injection to the TiO_2 surface.

Electrochemical impedance

The impact of anchoring groups on the same dyes (PCC *vs.* PRA) was further elucidated by electrochemical impedance spectroscopy (EIS). EIS is a useful technique to understand the important interfacial charge-transfer processes that occur in solar cells, such as the charge recombination at the TiO_2/dye/electrolyte interface, electron transport in the TiO_2 electrode, electron transfer at the counter electrode and I_3^- transport in

Published on 28 April 2016. Downloaded by University of California - Santa Barbara on 28/04/2016 11:19:50.

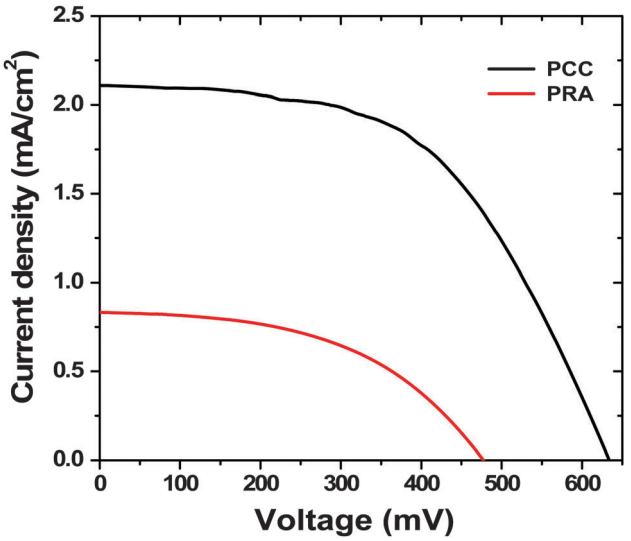

Fig. 9 *J–V* characteristics of the PCC and PRA devices.

Table 4 Photovoltaic properties of PCC and PRA devices

Dyes	Γ (mol cm^{-2})	J_{SC} (mA cm^{-2})	V_{OC} (V)	FF	η (%)	τ (ms)
PCC	18.31×10^{-7}	2.11	0.63	0.53	0.84	6.24
PRA	3.05×10^{-7}	0.83	0.47	0.50	0.23	3.22

the electrolyte.[82] The charge recombination dynamics between the injected electrons in TiO_2 and I_3^- in electrolyte competes with the charge collection process and limits both the V_{OC} and J_{SC}.[83–85] Thus, electrochemical impedance spectroscopy has been used to study this effect in the frequency domain. Fig. S28 (ESI†) shows the EIS Nyquist plots for DSCs based on PCC and PRA. Generally, the largest semicircle in the lower frequency range in the Nyquist plot represents the interfacial charge transfer at the TiO_2/dye/electrolyte interface,[83,84] which is the charge recombination between injected electrons and the electrolyte. Hence, the obtained plot in Fig. S28 (ESI†) looks like a semicircle which is assigned to the charge transfer resistance at the TiO_2/dye/electrolyte interface.

The diameter of the semicircle is higher for PCC and lower for PRA, which means that the electron transfer resistance for the unwanted back reaction is larger for PCC than that of PRA. This may be responsible for the achieved higher V_{OC} and J_{SC} of PCC. In Fig. S29 (ESI†), the frequency response plot is in the range 1–100 Hz, which is indicative of the electron recombination between the electrolyte and TiO_2 and is related to the electron lifetime in the CB of TiO_2. The electron lifetime depends on the density of charge traps, which is ultimately related to V_{OC}. Therefore, Bode phase plots (Fig. S29, ESI†) were used to find out the effective lifetime (τ_{eff}) of electrons in the conduction band of TiO_2. τ_{eff} was calculated[86] using eqn (6)

$$\tau_{eff} = 1/2\pi f \quad (6)$$

where, f is the frequency of the corresponding peak in the Bode phase plot. The obtained electron lifetimes for PCC and PRA are 6.24 and 3.22 ms, respectively. In principle, a longer electron lifetime indicates improved suppression of back reactions between the injected electrons and the electrolyte and leads to improvement of the V_{OC} value, due to the reduced electron recombination rate.[87] Consequently, the observed longer electron lifetime in the case of PCC could explain its high V_{OC} and also the higher efficiency as well as more effective suppression of back reactions compared to PRA. Hence, the EIS results provide evidence that the acceptor/anchoring unit plays a pivotal role in the overall efficiency of DSCs.

New insights from the present investigation

Although the pioneering work on the effect of electron withdrawing anchoring groups on the pyrene chromophore was reported by Paramaguru and co-workers,[88] the striking differences between the present and previous reports are discussed below. In their report, the five different anchoring groups were chosen and the photophysical properties and TiO_2 sensitization were studied. However, in the present work, we have meticulously engineered the pyrene chromophore using various anchoring groups. Detailed investigations of the relationship between the dye structures and photophysical, electrochemical and photovoltaic properties are described. The following points will clearly emphasise the novelty of our work.

We have systematically engineered the pyrene chromophore using anchoring groups with different electron withdrawing abilities. This kind of systematic approach will give an idea about 'how even a subtle change in the anchoring groups influences the ground and excited state properties of the pyrene chromophore'.

The effect of anchoring groups on the molecular geometry and electron density distribution of pyrene derivatives is investigated by quantum chemical calculations using five different functionals. B3LYP is found to predict the energy gap of the pyrene derivatives reasonably.

Both computational and spectroscopic studies show that by varying the anchoring groups a systematic bathochromic shift in the λ_{max} and λ_{emi} of pyrene derivatives was obtained.

The ICT nature of the pyrene derivatives was incontrovertibly demonstrated by using time resolved fluorescence spectroscopy.

Choosing an appropriate solvent for preparing the photoanode of a cell is of prime importance to obtain better power conversion efficiency. We have demonstrated that methanol is a suitable solvent for the sensitization process.

Photovoltaic measurements were performed on PCC and PRA dyes. PCC shows a better power conversion efficiency than PRA. We investigated the reason behind the inferior performance of PRA through FMO analysis.

A better photovoltaic performance of PCC is rationalized by a high surface coverage, efficient electron injection and a longer electron lifetime as demonstrated by the electrochemical impedance spectroscopy (EIS) measurements.

Our results suggest that, to achieve better excited state and photovoltaic properties of pyrene, an olefinic spacer is not adequate. In an extension of this work, we found that instead of the olefinic spacer, a rigid π-system improves the

Published on 28 April 2016. Downloaded by University of California - Santa Barbara on 28/04/2016 11:19:50.

stability of the dye as well as excited state properties, which will be report in a separate paper.

Conclusion

The objective of this work was to perform a systematic analysis of the absorption and emission characteristics and to explore the effect of anchoring groups. To fulfill this goal, we adopted the pyrene chromophore with various anchoring groups. Our results reveal that the absorption and emission properties of pyrene derivatives follow the sequence P < PC < PAC < PMC < PCC < PMN < PR < PRA, manifesting a clear anchoring group effect. For instance, the threshold wavelength of the absorption spectrum of PRA is 535 nm, while for pyrene it is 375 nm. Furthermore, the lifetimes of the first excited states (S_1) for ICT based dyes are estimated to be of the order of magnitude of 10^{-12} s, implying that these dyes can inject electrons into the semiconductor potentially. Upon dye adsorption, PCC and PRA molecules are found to be well adsorbed on the TiO_2 surface, this reveals that the dyes devised using cyanoacrylic acid and rhodanine-3-acetic acid may be promising sensitizers for DSCs. The overall conversion efficiencies of these dyes are not very high; however, this issue can be circumvented by realizing improvements in the synthetic route towards these dyes, such as the judicious introduction of a rigid ring system between the pyrene core and the anchoring group, this work is currently underway in our laboratory.

Acknowledgements

A. K., K. S. and M. J. thank Department of Science and Technology, India for DST-INSPIRE Faculty Award [IFA12-CH-78, IFA12-CH-35 and IFA13-CH-100]. We thank Mr G. Dhinagaran, NCUFP, Chennai, for his assistance in synthesis.

References

1 B. O'Regan and M. Grätzel, *Nature*, 1991, **353**, 737–740.
2 M. Gratzel, *Nature*, 2001, **414**, 338–344.
3 M. Gratzel, *Acc. Chem. Res.*, 2009, **42**, 1788–1798.
4 F. Gao, Y. Wang, J. Zhang, D. Shi, M. Wang, R. Humphry-Baker, P. Wang, S. M. Zakeeruddin and M. Grätzel, *Chem. Commun.*, 2008, 2635–2637.
5 J. H. Yum, I. Jung, C. Baik, J. Ko, M. K. Nazeeruddin and M. Grätzel, *Energy Environ. Sci.*, 2009, **2**, 100–102.
6 A. Mishra, M. K. Fischer and P. Bauerle, *Angew. Chem., Int. Ed.*, 2009, **48**, 2474–2499.
7 W. Xu, B. Peng, J. Chen, M. Liang and F. Cai, *J. Phys. Chem. C*, 2008, **112**, 874–880.
8 D. Patel, N. Bastianon, P. Tongwa, J. Leger, T. Timofeeva and G. Bartholomew, *J. Mater. Chem.*, 2011, **21**, 4242–4250.
9 M. V. Martínez-Díaz, G. de la Torre and T. Torres, *Chem. Commun.*, 2010, **46**, 7090–7108.
10 H. Imahori, T. Umeyama, K. Kurotobi and Y. Takano, *Chem. Commun.*, 2012, **48**, 4032–4045.
11 M. J. Griffith, K. Sunahara, P. Wagner, K. Wagner, G. Wallace, D. L. Officer, A. Furube, R. Katoh, S. Mori and A. J. Mozer, *Chem. Commun.*, 2012, **48**, 4145–4162.
12 L. L. Li and E. W. G. Diau, *Chem. Soc. Rev.*, 2013, **42**, 291–304.
13 T. Bessho, S. M. Zakeeruddin, C. Y. Yeh, E. W. G. Diau and M. Gratzel, *Angew. Chem., Int. Ed.*, 2010, **49**, 6646–6649.
14 A. Yella, H. W. Lee, H. N. Tsao, C. Yi, A. K. Chandiran, M. K. Nazeeruddin, E. W. G. Diau, C. Y. Yeh, S. M. Zakeeruddin and M. Gratzel, *Science*, 2011, **334**, 629–634.
15 S. Mathew, A. Yella, P. Gao, R. Humphry-Baker, B. F. E. Curchod, N. Astani, I. Tavernelli, U. Rothlisberger, M. K. Nazeeruddin and M. Gratzel, *Nature*, 2014, **6**, 242–247.
16 A. Hagfeldt, G. Boschloo, L. Sun, L. Kloo and H. Pettersson, *Chem. Rev.*, 2010, **110**, 6595–6663.
17 H. N. Tsao, J. Burschka, C. Yi, F. Kessler, M. K. Nazeeruddin and M. Gratzel, *Energy Environ. Sci.*, 2011, **4**, 4921–4924.
18 W. D. Zeng, Y. M. Cao, Y. Bai, Y. H. Wang, Y. S. Shi, M. Zhang, F. F. Wang, C. Pan and P. Wang, *Chem. Mater.*, 2010, **22**, 1915–1925.
19 A. Harriman, G. Izzet and R. Ziessel, *J. Am. Chem. Soc.*, 2006, **128**, 10868–10875.
20 S. W. Yang, A. Elangovan, K. C. Hwang and T. I. Ho, *J. Phys. Chem.*, 2005, **109**, 16628–16635.
21 J. M. Casas-Solvas, J. D. Howgego and A. P. Davis, *Org. Biomol. Chem.*, 2014, **12**, 212–232.
22 T. M. Figueira-Duarte and K. Muellen, *Chem. Rev.*, 2011, **111**, 7260–7314.
23 G. Drummen, *Molecule*, 2012, **17**, 14067–14090.
24 A. M. Breul, M. D. Hager and U. S. Schubert, *Chem. Soc. Rev.*, 2013, **42**, 5366–5407.
25 J. Zhao, W. Wu, J. Sun and S. Guo, *Chem. Soc. Rev.*, 2013, **42**, 5323–5351.
26 M. E. Ostergaard and P. J. Hrdlicka, *Chem. Soc. Rev.*, 2011, **40**, 5771–5788.
27 N. Joong Jeon, J. Lee, J. H. Noh, M. K. Nazeeruddin, M. Grätzel and S. Seok, *J. Am. Chem. Soc.*, 2013, **135**, 19087–19090.
28 H. U. Kim, J. H. Kim, H. Kang, A. C. Grimsdale, B. J. Kim, S. C. Yoon and D. H. Hwang, *ACS Appl. Mater. Interfaces*, 2014, **6**, 20776–20785.
29 S. Y. Liu, W. Q. Liu, J. Q. Xu, C. C. Fan, W. F. Fu, J. Ling, J. Y. Wu, M. M. Shi, A. K. Jen and H. Z. Chen, *ACS Appl. Mater. Interfaces*, 2014, **6**, 6765–6775.
30 O. Taratula, J. Rochford, P. Piotrowiak, E. Galoppini, R. A. Carlisle and G. J. Meyer, *J. Phys. Chem. B*, 2006, **110**, 15734–15741.
31 D. Kumar, K. R. Justin Thomas, C. P. Lee and K. C. Ho, *Org. Lett.*, 2011, **13**, 2622–2625.
32 A. Baheti, C. P. Lee, K. R. Justin Thomas and K. C. Ho, *Phys. Chem. Chem. Phys.*, 2011, **13**, 17210–17211.
33 K. R. Justin thomas, N. Kapoor, C. P. Lee and K. C. Ho, *Chem. – Asian J.*, 2012, **7**, 738–750.
34 J. Huang, K. Jiang, C. C. Yu, S. G. Li, L. M. Yang and Y. L. Song, *RSC Adv.*, 2014, **4**, 22181–22185.
35 S. S. Li, K. J. Jiang, C. C. Yu, J. H. Huang, L. M. Yanga and Y. L. Song, *New J. Chem.*, 2014, **38**, 4404–4408.

Published on 28 April 2016. Downloaded by University of California - Santa Barbara on 28/04/2016 11:19:50.

36 C. L. Wang, Y. C. Chang, C. M. Lan, C. F. Lo, E. W. G. Diau and C. Y. Lin, *Energy Environ. Sci.*, 2011, **4**, 1788–1795.
37 M. Katono, T. Bessho, M. Wielopolski, M. Marszalek, J. E. Moser, R. H. Baker, S. M. Zakeeruddin and M. Grätzel, *J. Phys. Chem. C*, 2012, **116**, 16876–16884.
38 F. Ambrosio, N. Martsinovich and A. Troisi, *J. Phys. Chem. Lett.*, 2012, **3**, 1531–1535.
39 S. Karthikeyan and J. Y. Lee, *J. Phys. Chem. A*, 2013, **117**, 10973–10979.
40 L. Zhang and J. M. Cole, *ACS Appl. Mater. Interfaces*, 2015, **7**, 3427–3455.
41 J. Wiberg, T. Marinado, D. P. Hagberg, L. Sun, A. Hagfeldt and B. Albinsson, *J. Phys. Chem. C*, 2009, **113**, 3881–3886.
42 G. Wu, F. Kong, J. Li, W. Chen, X. Fang, C. Zhang, Q. Chen, X. Zhang and S. Dai, *Dyes Pigm.*, 2013, **99**, 653–660.
43 Z. Li, M. Smeu, M. A. Ratner and E. Borguet, *J. Phys. Chem. C*, 2013, **117**, 14890–14898.
44 O. Taratula, J. Rochford, P. Piotrowiak, E. Galoppini, R. A. Carlisle and G. J. Meyer, *J. Phys. Chem. B*, 2006, **110**, 15734–15741.
45 D. F. Eaton, *Pure Appl. Chem.*, 1988, **60**, 1107–1114.
46 K. Suzuki, A. Kobayashi, S. Kaneko, K. Takehira, T. Yoshihara, H. Ishida, Y. Shiina, S. Oishic and S. Tobita, *Phys. Chem. Chem. Phys.*, 2009, **11**, 9850–9860.
47 J. Shen and R. D. Snook, *Chem. Phys. Lett.*, 1989, **155**, 583–586.
48 A. D. Becke, *J. Chem. Phys.*, 1993, **98**, 5648–5652.
49 C. Lee, W. Yang and R. G. Parr, *Phys. Rev. B: Condens. Matter Mater. Phys.*, 1988, **37**, 785–789.
50 J. P. Perdew, K. Burke and M. Ernzerhof, *Phys. Rev. Lett.*, 1997, **78**, 1396.
51 M. Ernzerhof and G. E. Scuseria, *J. Chem. Phys.*, 1999, **110**, 5029–5034.
52 C. Adamo and V. Barone, *J. Chem. Phys.*, 1999, **110**, 6158–6169.
53 Y. Zhao and D. G. Truhlar, *Theor. Chem. Acc.*, 2008, **120**, 215–241.
54 J.-D. Chai and M. Head-Gordon, *Phys. Chem. Chem. Phys.*, 2008, **10**, 6615–6620.
55 E. Runge and E. K. U. Gross, *Phys. Rev. Lett.*, 1984, **52**, 997–1000.
56 A. Dreuw and M. Head-Gordon, *Chem. Rev.*, 2005, **105**, 4009–4037.
57 J. Tomasi and M. Persico, *Chem. Rev.*, 1994, **94**, 2027–2094.
58 V. Barone, M. Cossi and J. Tomasi, *J. Comput. Chem.*, 1998, **19**, 404–417.
59 M. Frisch, *et al.*, *Gaussian 09, Revision D. 01*, Gaussian, Inc., Wallingford, CT, 2010.
60 N. Pavithra, A. Asiri and S. Anandan, *J. Power Sources*, 2015, **286**, 346–353.
61 W. Xu, B. Peng, J. Chen, M. Liang and F. Cai, *J. Phys. Chem. C*, 2008, **112**, 874–880.
62 S. K. Pal, V. Sundstrom, E. Galoppini and P. Persson, *Dalton Trans.*, 2009, 10021–10031.
63 H. Örücü and N. Acar, *Comput. Theor. Chem.*, 2015, **1056**, 11–18.
64 X. Feng, J. Y. Hu, X. F. Wei, C. Redshaw and T. Yamato, *J. Mol. Struct.*, 2015, **1086**, 216–222.
65 B. H. Kim and H. S. Freeman, *Dyes Pigm.*, 2013, **96**, 313–318.
66 R. L. Martin, *J. Chem. Phys.*, 2003, **118**, 4775–4776.
67 J. Feng, Y. Jiao, W. Ma, Md. K. Nazeeruddin, M. Grätzel and S. Meng, *J. Phys. Chem. C*, 2013, **117**, 3772–3778.
68 D. Kuang, S. Ito, B. Wenger, C. Klein, J. E. Moser, R. H. Baker, S. M. Zakeeruddin and M. Grätzel, *J. Am. Chem. Soc.*, 2006, **128**, 4146–4154.
69 F. M. Winnik, *Chem. Rev.*, 1993, **93**, 587–614.
70 M. Grätzel, *J. Photochem. Photobiol., C*, 2003, **4**, 145–153.
71 Z. R. Grabowski, K. Rotkiewicz and W. Rettig, *Chem. Rev.*, 2003, **103**, 3899–4032.
72 A. Baheti, P. Tyagi, K. R. J. Thomas, Y. C. Hsu and J. T. Lin, *J. Phys. Chem. C*, 2009, **113**, 8541–8547.
73 B. Venkatachalapathy and P. Ramamurthy, *Phys. Chem. Chem. Phys.*, 1999, **1**, 2223–2230.
74 A. Baheti, S. R. Gajjela, P. Balaya and K. R. J. Thomas, *Dyes Pigm.*, 2015, **113**, 78–86.
75 R. Jono, J. Fujisawa, H. Segawa and K. Yamashita, *Phys. Chem. Chem. Phys.*, 2013, **15**, 18584–18588.
76 T. Marinado, D. P. Hagberg, M. Hedlund, T. Edvinsson, E. M. J. Johansson, G. Boschloo, H. Rensmo, T. Brinck, L. Sun and A. Hagfeldt, *Phys. Chem. Chem. Phys.*, 2009, **11**, 133–141.
77 K. Kalyanasundaram and J. K. Thomas, *J. Am. Chem. Soc.*, 1977, **99**, 2039–2044.
78 A. Cidlina, V. Novakova, M. Miletina and P. Zimcik, *Dalton Trans.*, 2015, **44**, 6961–6971.
79 O. Bräm, A. Cannizzo and M. Chergui, *Phys. Chem. Chem. Phys.*, 2012, **14**, 7934–7937.
80 K. M. Lee, V. Suryanarayanan and K. C. Ho, *J. Power Sources*, 2009, **188**, 635–641.
81 J. H. Mecchia Ortiz, C. Longo and N. E. Katz, *Inorg. Chem. Commun.*, 2015, **55**, 69–72.
82 Q. Wang, J. E. Moser and M. Grätzel, *J. Phys. Chem. B*, 2005, **109**, 14945–14953.
83 N. Koide, A. Islam, Y. Chiba and L. Y. J. Han, *J. Photochem. Photobiol., A*, 2006, **182**, 296–305.
84 F. Fabregat-Santiago, G. Garcia-Belmonte, I. Mora-Sero and J. Bisquert, *Phys. Chem. Chem. Phys.*, 2011, **13**, 9083–9118.
85 K. Pei, Y. Z. Wu, A. Islam, Q. Zhang, L. Y. Han, H. Tian and W. H. Zhu, *ACS Appl. Mater. Interfaces*, 2013, **5**, 4986–4995.
86 D. D. Babu, S. R. Gachumale, S. Anandan and A. V. Adhikari, *Dyes Pigm.*, 2015, **112**, 183–191.
87 D. Kuang, S. Uchida, R. Humphry-Baker, S. M. Zakeeruddin and M. Gratzel, *Angew. Chem., Int. Ed.*, 2008, **47**, 1923–1927.
88 G. Paramaguru, R. Vijay Solomon, S. Jagadeeswari, P. Venuvanalingam and R. Renganathan, *J. Photochem. Photobiol., A*, 2013, **271**, 31–44.

 This journal is © the Owner Societies 2016